Applied Surface Science 638 (2023) 158032

Contents lists available at ScienceDirect

Applied Surface Science

journal homepage: www.elsevier.com/locate/apsusc

Full Length Article

Tailoring the wettability of surface-textured copper using sub-THz bursts of femtosecond laser pulses

Caterina Gaudiuso [a,b,*], Fiorenza Fanelli [c], Francesco Paolo Mezzapesa [a], Annalisa Volpe [a,b], Antonio Ancona [a,b]

[a] National Research Council (CNR), Institute for Photonics and Nanotechnologies (IFN), Via G. Amendola, 173, 70125 Bari, Italy
[b] Intercollegiate Department of Physics "M. Merlin", University of Bari and Polytechnic University of Bari, Via G. Amendola 173, 70125 Bari, Italy
[c] National Research Council (CNR), Institute of Nanotechnology (NANOTEC), via Orabona 4, 70125 Bari, Italy

ARTICLE INFO

Keywords:
Laser surface structuring
LIPSS
One-step hierachical morphology
Femtosecond laser pulse bursts
Laser-induced surface chemistry
Wettability

ABSTRACT

In this work, copper surfaces were textured with sub-Terahertz bursts of femtosecond pulses. The wettability of Cu textured surfaces was investigated by measuring the static water contact angle (WCA) as a function of the number of sub-pulses and the intra-burst frequency. A superhydrophobic, antiadhesive response was observed when using bursts with a high number of sub-pulses (equal to or higher than 16) or a high intra-burst frequency (equal to or higher than 0.09 THz). Such trend was ascribed to the generation, under specific laser irradiation conditions, of a double-scale hierarchical texture on the sample surface, formed by sub-micro patterns with fine periodic ripples (LIPSS, Laser-Induced Periodic Surface Structures) and random nanoparticle decoration. Such texture enhances the hydrophobic behavior given by inherent adsorption of adventitious hydrocarbons on laser-processed and thermally-treated metal targets.

1. Introduction

Leveraging laser surface functionalization to control single-step generation of bionic superhydrophobicity is expected to foster innovation towards practical applications in various fields, including medicine, sensing, mechanics, biotechnology [1–4].

Ultrafast laser structuring in the micro- and nanometer range is by far the most sustainable fabrication method for producing surfaces with morphology-sensitive wettability on common metals [5–10], as neither specific chemicals nor waste are involved. It has been shown that pure metallic surfaces exhibit tailored superhydrophobic and adhesion properties when directly irradiated with nano- and femtosecond laser pulses, and that optimal surface functionalization relies upon both the topographic modification and the alteration of surface energy during/after laser patterning.

Periodic 1D/2D sub-wavelength Laser-Induced Periodic Surface Structures (LIPSS), self-generated on metals by trains and/or bursts of GHz and THz ultrashort laser pulses [11–16], are known to provide naïve wetting response and special adhesion to the surface without any additional treatment. Moreover, if superimposed to the riblet structures in a multiscale morphology fashion, they can effectively induce superhydrophobic nature characterized by very low values of both rolling-off angle and contact angle hysteresis [17].

The wetting response of rough solid targets is generally described through Wenzel or Cassie-Baxter model [18] depending on whether their surface protrusions are filled by the liquid or if they rather form pockets where air can be trapped and sustain the liquid drops. However, the final wettability of complex structured surfaces is often far from being easy to predict. Nevertheless, thanks to its versatility, laser surface structuring has the potential to unveil the correlations between surface morphology and wettability, owing to its capability to generate a wide range of surface structures on different size scale [3,11–15,19,20]. In particular, while it is known that, right after the laser treatment, textured samples are generally superhydrophilic, the wetting response shifts to a stable hydrophobic or superhydrophobic character, depending on the surface morphologies induced by the laser irradiation conditions [11].

In [3], direct laser writing was exploited to generate square, circular and triangular patterns on aluminum alloy AA2024, showing that for superhydrophobicity to be reached, it was generally necessary to increase the textured area from ca 20% up to 60% (triangular and circular lattice) or 80% (square lattice), which resulted in a detectable increase

* Corresponding author.
E-mail address: caterina.gaudiuso@cnr.it (C. Gaudiuso).

https://doi.org/10.1016/j.apsusc.2023.158032
Received 22 March 2023; Received in revised form 28 June 2023; Accepted 12 July 2023
Available online 13 July 2023

of the processing time.

In [21], 316L steel samples were textured with four different patterns, i.e., nano-rippled, parabolic-pillared, elongated sinusoidal-pillared and triple roughness nano-structures. Irrespective of the pattern, the enhancement of the hydrophobic behavior was linked to the increase of the accumulated fluence, due to a modulation of the structures depth and periodicity. A similar trend was also found in [17] on Ti-6Al-4 V, where the authors also showed that hierarchical structures with an even more pronounced hydrophobic character could be obtained by a double step process consisting of generating LIPSS overlapped to directly laser written microstructures.

Among metals, copper is the most widely used for electronics and industrial devices and known to be highly reactive in air atmosphere. Therefore, is is easily affected by environmental conditions (i.e. humidity) leading to oxidation, fouling, and ice accretion. In agreement with what was previously reported on other metals, laser texturing of copper targets can result in changes of the wetting response ascribed to surface roughness [22,23] induced by nanosecond laser pulses/treatment(even though durable superhydrophobicity was subordinated to organic-compound-assisted annealing at low temperature [24,25].) The wetting response of copper surface was also correlated to the multi-scale hierarchical morphology demonstrated by femtosecond laser texturing in air, attributing the progressive increase of the superhydrophobic character to the laser pulse fluence and to the consequent combined effect of ripples and nanoparticles/nanobumps upon the textured surface [8,26].

From the previous discussion, it is clear that multi-step processing, higher fluence and/or longer processing times are required to obtain superhydrophobicity and antiadhesiveness response. In this work, we propose an alternative strategy, based on using burst mode (BM) processing. While many works exploited bursts of THz ultrashort laser pulses for studying the laser-matter interaction processes [27–30] and surface structuring of metal targets [11], to the best of the authors' knowledge, this is the first time that a systematic study has been carried out to elucidate the effect of burst features on the wetting response of the laser-treated materials in burst mode (BM), as well as to identify novel strategies to finely tune the wettability from hydrophobicity to superhydrophobicity.

Here, we report on an experimental investigation of the tailorability and origin of copper wettability, by generating LIPSS with bursts of 200-fs-pulses in the sub-THz intra-burst frequency regime, with no further increase of the laser fluence nor use of chemical compounds to attribute special wetting properties to the structured samples. The burst features were varied to highlight the influence of the number of pulses (from 2 to 32) and the intra-burst frequency (from 0.02 THz up to 0.67 THz) on surface morphology and chemistry. SEM and XPS analysis allowed identifying the main factors that are responsible for the final wettability of the processed samples.

2. Experimental set-up

2.1. Laser induced periodic surface structures (LIPSS) generation with bursts

LIPSS were generated on copper targets by means of a Pharos 1.5-SP laser from Light Conversion, emitting 200-fs (FWHM) horizontally polarized pulses at 1030 nm of central wavelength. A burst generator consisting of five birefringent (calcite) crystals was used to produce a burst from each pulse exiting the laser source [28,31,32]. Depending on the mutual orientation of the pulses and the optical axes of the calcite crystals, it was possible to split the incoming laser pulse into *n* sub-pulses (n from 2 to 32) having equal fractioned energy. The intra-burst frequency also depends both on the crystal orientation and thickness, and it was set to 0.67 THz, 0.34 THz, 0.22 THz, 0.17 THz, 0.09 THz, 0.03 THz and 0.02 THz. The crossed polarized sub-pulses emerging form the burst generator [16] were converted into vertical polarized with a polarizer oriented at ± 45° to the emerging polarizations of the sub-pulses and place right after the calcite crystals cascade. Therefore, in order to have the polarization of all the sub-pulses aligned, half of the available power was cut by the polarizer. The fluence of the whole bursts was set at 0.52 J/cm^2 by placing a half waveplate followed by a polarizer right before the burst generator.

Laser surface structuring was carried out in ambient air by scanning, on the copper targets, horizontal lines separated by a hatch *h* of 1 μm, using a galvo-scanner (SCANLAB's IntelliSCAN 14) equipped with a 56-mm focal length F-Theta telecentric lens. The laser beam diameter *d* focused on the sample surface was 24 μm ± 1 μm (1/e^2 peak intensity), as measured with a CCD camera (FireWire BeamPro Model 2523 by Photon Inc.). The laser repetition rate was set at 200 kHz to ensure high processing speed (0.9 m/s) over the 10 × 5 mm^2 scanned area.

Once the processing parameters and the total fluence were set, surface structuring experiments were performed with different burst configurations, in order to highlight the influence of the laser energy distribution within the bursts and to study how it affected the suface morphology and chemistry. In fact, varying the burst configuration does not change the total energy load impinging on the targets, but rather the way how such laser energy is delivered/provided to the samples. This aspect is clearly shown in Table 1, where the burst configurations used for the structuring experiments are summarized.

After the laser surface treatment, the processed samples were kept at 120 °C for 3 h. The low temperature annealing was performed to accelerate the transition from hydrophilicity to hydrophobicity [33] and to settle the wetting response [11]. In fact, an aging period (whose duration depends on the material) is usually necessary to stabilize the wettability of a laser treated surface. During the aging period in ambient air, the surface chemistry changes and usually enriches with hydrocarbons and oxides. In order to speed up this process, we carried out the thermal treatment, as suggested also in [2]. This procedure allowed exploiting the samples almost immediately after the laser treatment, with no need to wait for the aging period (tens of days) to stabilize their wettability [34].

2.2. Surface characterization

The morphology of the laser structured samples was investigated using a Σigma scanning electron microscope (SEM) from Zeiss. The SEM images were analyzed by means of a free source software (Gwyddion) for performing the Fast Fourier Transform and retrieving the LIPSS period.

Surface chemistry was investigated by X-ray photoelectron spectroscopy (XPS) using a PHI 5000 Versa Probe II Scanning XPS

Table 1
Burst configurations exploited in the structuring experiments. The configurations used for the analysis of the surface morphology discussed in section 3.1 and 3.2 are explicitly pointed out in bold and sketched in Fig. 1. Here, n is the number of sub-pulses in the bursts, f_b is the intra-burst frequency and the burst duration is defined as the total time duration of a burst, given by (n-1)*1/f_b.

Burst Configuration		Burst Duration (ps)	Total Fluence F_b (J/cm^2)	Sub-pulse fluence F_{sp} (J/cm^2)
n	f_b (THz)			
2	**0.67**	**1.5**	**0.52**	**0.26**
	0.34	3		
	0.22	4.5		
	0.17	6		
	0.09	10.5		
	0.03	36		
	0.02	**46.5**		
4	**0.67**	4.5	**0.52**	0.13
8		10.5		0.065
16		22.5		0.0325
32		**46.5**		**0.01625**

Microprobe spectrometer (ULVAC-PHI Inc., Kanagawa, Japan). Measurements were carried out with a monochromatised Al Kα source (source energy = 1486.6 eV, spot size = 100 μm) at a power of 24.8 W. Overall and high-resolution spectra were acquired in fixed analyzer transmission (FAT) mode with a pass energy of 117.40 eV and 23.50 eV, respectively, at a take-off angle of 45° with respect to the sample normal. Dual-beam charge neutralization was used during the analysis for charge compensation. The binding energy (BE) scale was corrected taking the hydrocarbon component of the C 1 s spectrum at 284.8 ± 0.1 eV as reference. Data processing was performed by using the MultiPak software v. 9.5.0.8 (ULVAC-PHI Inc.).

The influence of the different burst configurations on the surface properties was evaluated by characterizing the surface wetting response, measuring the static water contact angle (WCA) on the laser-structured samples (after the thermal treatment). For this purpose, a digital goniometer was used, which consisted of a Dino-lite portable microscope combined with a lamp for back-lighting of the drop (5 μl bidistilled water). The unprocessed, thermally-treated sample was also characterized for comparison.

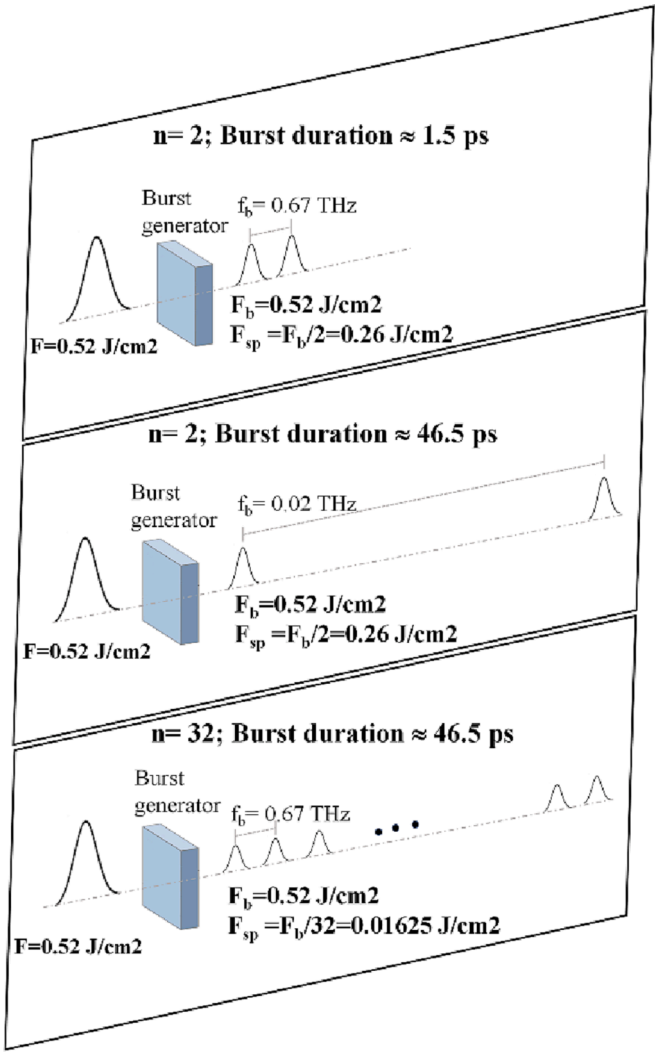

Fig. 1. Sketch of the main three burst configurations exploited in the present work.

3. Results and discussion

3.1. LIPSS morphology with different burst configurations

In Fig. 2, the different morphologies obtained by using bursts with three different features (n = 2 and f_b = 0.67 THz, n = 32 and f_b = 0.67 THz, and n = 2 and f_b = 0.02 THz) but equal total fluence (0.52 J/cm^2) are shown. As mentioned in section 2.1, the processing parameters, i.e., scan speed, hatch distance, and repetition rate, were set to be the same for all the structuring experiments. Therefore, using different bursts configurations resulted in a different distribution of the total laser pulse energy among the sub-pulses of the bursts but the total energy delivered per unit surface does not change.

As expected, being the polarization of all the sub-pulses within the bursts vertical, the obtained morphologies consist of horizontal Low Spatial Frequency LIPSS (LSFL). Performing the Fast Fourier Transform (FFT) of the SEM images revealed that they were characterized by a slightly different spatial period. In fact, using bursts of two sub-pulses at 0.67 THz, LSFLs with a period of 891 ± 3 nm were generated, while, increasing the duration of the whole bursts, i.e., n = 32 @ 0.67 THz or n = 2 @ 0.02 THz, the spatial period settled on 912 ± 4 nm and 928 ± 10 nm, respectively, in good agreement with the results that had been previously reported on steel [16]. In one of our previous work [16], we observed a similar increasing trend of the period of the LIPSS as a function of the time delay and the number of pulses within the burst and a concomitant reduction of the LSFL depth. This depth reduction could explain, in agreement with [35], the concurrent increase of the LIPSS period. In fact, reducing the LIPSS depth could influence the coupling of the laser radiation with the surface plasmon polariton, leading to a shift in the LSFL period. However, we believe that for the physical mechanism behind this effect to be unveiled, some further investigations are needed.

Besides the different spatial periodicity of the LSFL, the zoomed images presented in Fig. 2 allow highlighting other significant peculiarities which arise with different burst features. In fact, while all of the three surfaces shown in Fig. 2 displayed some nanoparticles and/or nanoformations decorating the LIPSS, their presence was much more significant for structures generated by bursts with a duration of 46.5 ps. The formation of such nanoparticles is commonly ascribed to the interplay between thermal effects and redeposition of laser ablated particles [36]. In the present case, since the lattice thermalization after the absorption of the laser energy occurs after several picoseconds (the electron–phonon coupling τ_{el} in copper is 1–4 ps [37]), it is possible to assume that no initiation of the lattice decomposition occurs during 1.5 ps-long bursts (2-sub-pulses at 0.67 THz). Conversely, in case of longer bursts (n = 32 @ 0.67 THz or n = 2 @ 0.02 THz) the lattice expansion already occurs within the burst itself [11,38,39], causing the substrate to melt and making the formation of nanoparticles/nanocluster more likely.

In Fig. 3, the SEM images of an 8 × 11 μm2 area further highlight this behavior, also through the analysis of the Fast Fourier Transform (FFT). In the figure, it is clearly visible that bursts of two sub-pulses at an intra-burst frequency of 0.67 THz generated LIPSS with sparse nanoparticles/clusters decoration. The FFT of the corresponding SEM image shown in Fig. 3 a) presents two peaks in quite a dark background, which indicates that the regular and periodic structures prevail on other superimposed formations. Conversely, the FFT of the morphologies obtained with bursts configurations of 32 sub-pulses @ 0.67 THz and 2 sub-pulses @ 20 THz displayed a brigh cloud around the two peaks indicating the spatial frequencies of the LSFL. This confirms the presence of finer irregular nanoformations superimposed to the LSFL, with neither a clear periodicity nor a specific orientation. Such additional structures provided a double-scale (hierarchical) morphology to the surface topography. A further analysis of these three SEM images allowed evaluating the percentage of the surface covered by such finer nanoformations in the three main burst configurations. In particular, we found that for the surface in Fig. 3 a), i.e., n = 2 @ 0.67 THz, the surface coverage was approximately

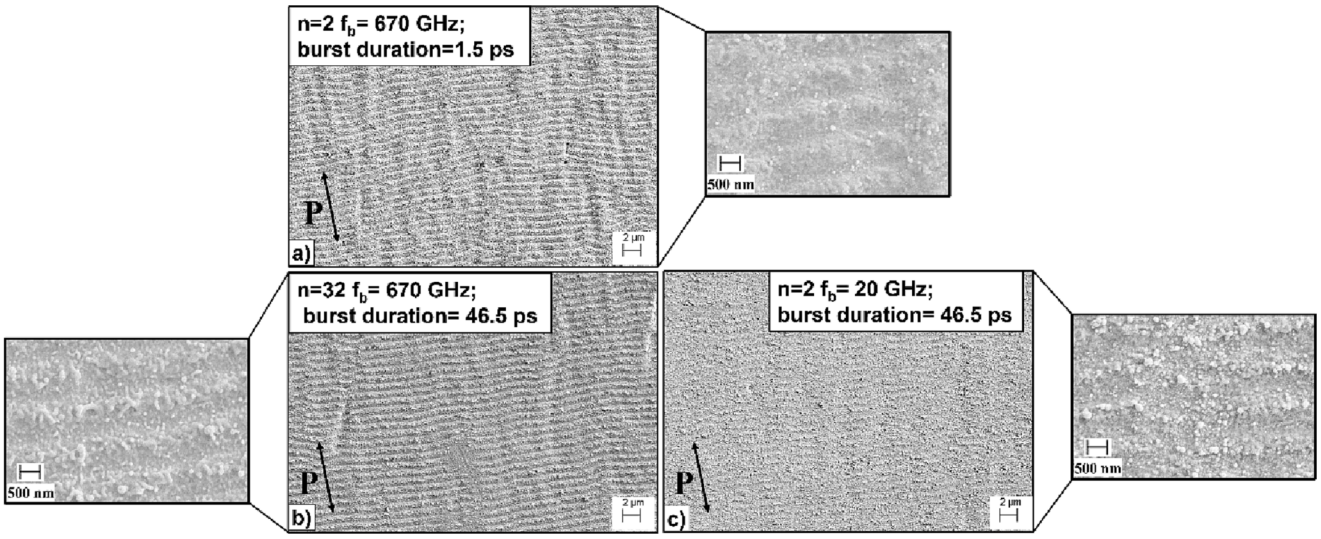

Fig. 2. Exemplary LIPSS morphologies obtained with bursts of a) 2 sub-pulses at an intra-burst frequency of 0.67 THz, b) 32 sub-pulses at an intra-burst frequency of 0.67 THz, and c) 2 sub-pulses at an intra-burst frequency of 0.02 THz.

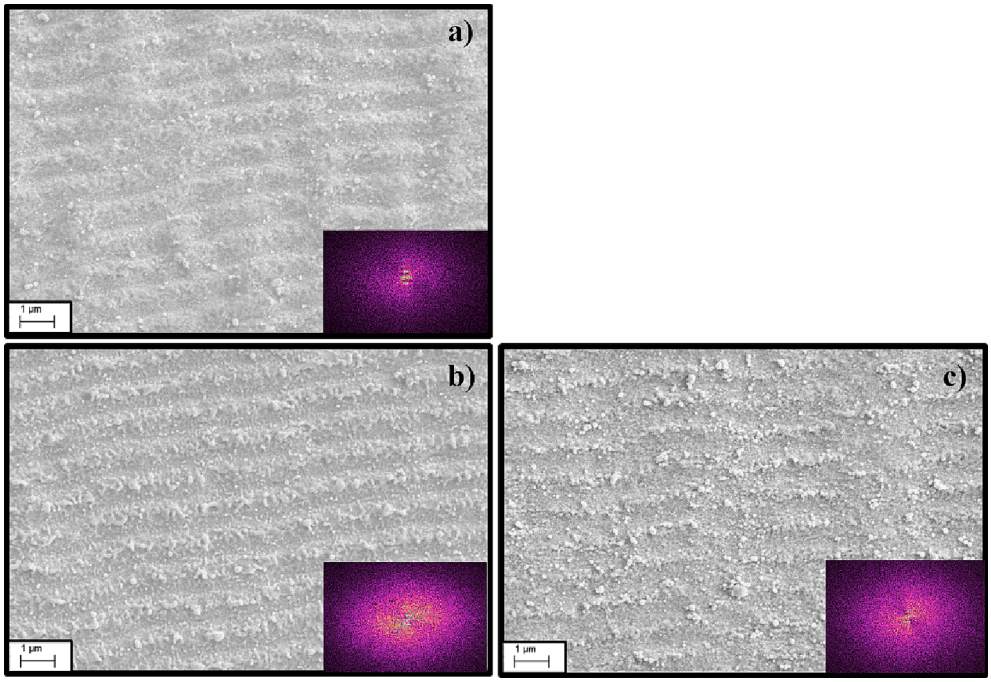

Fig. 3. SEM and corresponding FFT images of the morphologies obtained with bursts of a) 2 sub-pulses @ 0.67 THz, b) 32 sub-pulses @ 0.67 THz, and 2 sub-pulses @ 0.02 THz.

equal to 10%, while it was around 24% and 23% for the other two burst configurations, i.e., n = 32 @ 0.67 THz and n = 2 @ 0.02 THz, respectively.

From the previous morphological analysis it is clear that the burst duration strongly affects the final topography of the structured samples, especially when it is much longer than the electron–phonon coupling time τ_{el} (e.g., for bursts with a duration of 46.5 ps, ten times longer than τ_{el}). Nonetheless, also the sub-pulse fluence has a role. In fact, Fig. 4, where the surface morphologies obtained with bursts of 8 sub-pulses @ 0.67 THz (see Fig. 4 a)) and 2 @ 0.09 THz (see Fig. 4 b)) are shown, highlights how the nanoparticles/clusters generation was more inhibited when the sub-pulses in the burst are less energetic, though such bursts have the same time duration (10.5 ps) and total fluence. A more fractioned sub-pulse fluence (when n = 8@0.67 THz), i.e., four times less than for 2-sub-pulses@0.09 THz, reduces the melting within the duration of the burst (longer but still comparable with the τ_{el}). Therefore, the consequent formation of nanoparticles was mitigated by the much smaller temperature increase due to each sub-pulse of the burst. Later on, (Fig. 7 a) and b), section 3.3) it will be shown that this also resulted in a different wetting response.

3.2. *Surface chemistry of copper targets structured with different laser burst configurations*

The surface chemical composition of the laser-processed copper targets was investigated by XPS and compared with that of an unprocessed sample. The overall XPS spectra in Fig. 5 confirm the presence of carbon, oxygen and copper on both a thermally-treated unprocessed Cu

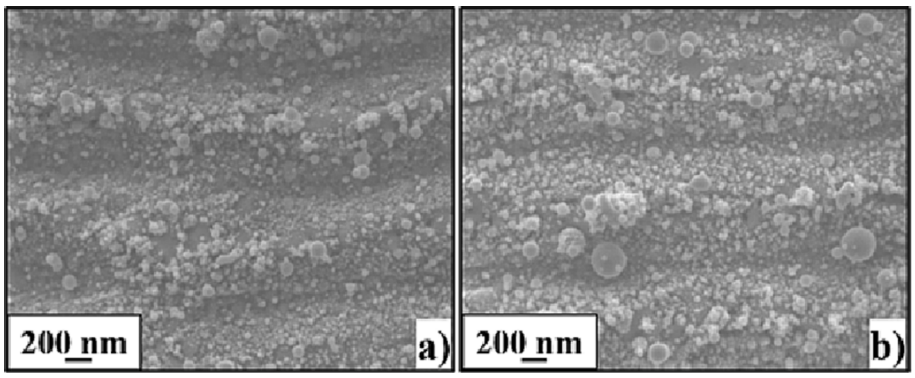

Fig. 4. SEM image of LSFL generated with bursts of a) 8 sub-pulses @ 0.67 THz and b) 2 sub-pulses @ 0.09 THz.

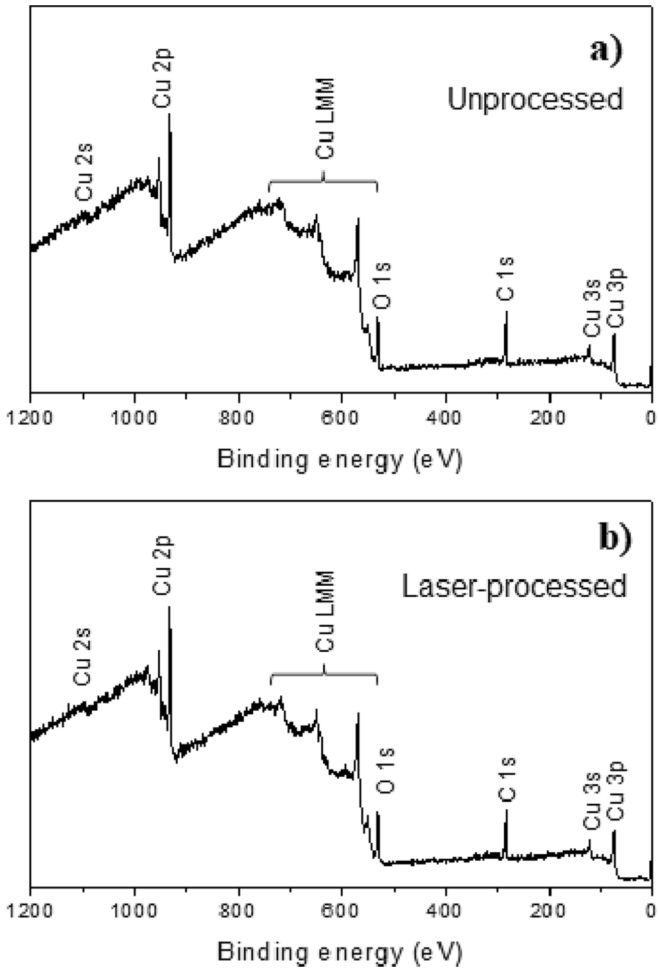

Fig. 5. Overall XPS spectra of a) a thermal-treated unprocessed Cu sample and b) a representative thermal-treated laser-processed Cu target (burst configuration with 2 sub-pulses at an intra-burst frequency of 0.67 THz).

sample and a representative thermally-treated laser-processed target (n = 2 and f_b = 0.67 THz). Table 2 reports the surface atomic concentrations of an unprocessed and three different laser-structured targets (after thermal treatment) determined from the high-resolution XPS spectra of C 1 s, O 1 s, and Cu $2p_{3/2}$ core levels. All samples present similar surface composition. In particular, Table 2 shows that the thermally-treated unprocessed sample is characterized by XPS atomic concentrations of C, O and Cu of 47%, 28% and 25%, respectively. In addition, results for the laser-processed targets evidence that the use of three different burst-configurations (n = 2 at f_b = 0.67 THz, n = 32 at f_b = 0.67 THz, and n = 2 at f_b = 0.02 THz) only induces a very slight decrease of the C atomic percentage (41–43%) and a concomitant increase of the O (30–33%) and Cu (26–27%) concentrations.

Table 2
XPS surface composition of a thermally-treated unprocessed Cu sample and three different thermally-treated laser-processed Cu targets obtained with bursts of 2 sub-pulses @ 0.67 THz, 32 sub-pulses @ 0.67 THz, 2 sub-pulses @ 0.02 THz.

Sample	C (at %)	O (at %)	Cu (at %)
Unprocessed	47 ± 3	28 ± 2	25 ± 2
Processed – n = 2, f_b = 0.67 THz	43 ± 2	30 ± 2	27 ± 2
Processed – n = 2, f_b = 0.02 THz	41 ± 2	33 ± 2	26 ± 2
Processed – n = 32, f_b = 0.67 THz	43 ± 2	31 ± 2	26 ± 2

Fig. 6 reports the high-resolution XPS spectra of the C 1 s, O 1 s, Cu $2p_{3/2}$ core levels and of the Cu $L_3M_{4,5}M_{4,5}$ (hereafter, referred to as Cu LMM) Auger transition of three different laser-structured targets and the unprocessed one after thermal treatment. The high-resolution C 1 s spectra of all samples are very similar and present the typical lineshape reported for adventitious carbon surface contamination [11,40]. They can be curve-fitted with the dominant hydrocarbon component (C − C, C − H; 284.8 ± 0.1 eV; ~85%) and two weak peaks due to C-O (286.3 ± 0.2 eV) and COO (288.7 ± 0.3 eV) groups (as a whole, ~15%). It is worth mentioning that the formation of an adventitious hydrocarbon-rich layer naturally occurs on freshly laser-irradiated metal surfaces upon long-term sample exposure to ambient atmosphere, and can be accelerated by low-temperature annealing as reported in prior studies and in this work [11,41].

The careful examination of the Cu $2p_{3/2}$ and Cu LMM spectra in Fig. 6 provides indications on the chemical state of copper on the samples' surface. First of all, the main peak of the Cu $2p_{3/2}$ spectra of all analysed samples can be curve-fitted with three components. In particular, the component at 932.3 ± 0.2 could be due to both Cu(0) and Cu(I) oxide (Cu_2O), while the two peaks centered at 933.6 ± 0.2 eV and 935.0 ± 0.2 eV can be assigned to Cu(II) species, such as Cu(II) oxide (CuO) and Cu (II) hydroxide $Cu(OH)_2$ (Fig. 5) [42–44]. The well-detectable shake-up peaks (938–947 eV) confirm the presence of Cu(II) species [42–44]. For all samples, the position of the Cu LMM Auger signal (binding energy, BE = 569.7 ± 0.2 eV; kinetic energy, KE = 916.9 ± 0.2 eV) and the modified Auger parameter (1849.2 ± 0.2 eV, determined as the sum of the Cu $2p_{3/2}$ signal BE and the Cu LMM signal KE) suggest that Cu(0) is not present in appreciable amount on the targets' surface and allow assigning the Cu $2p_{3/2}$ component at 932.3 ± 0.2 eV predominantly to Cu_2O [42–44]. It can be therefore concluded that copper is mainly present on the surface of the thermally-treated unprocessed and processed targets as Cu_2O, CuO and $Cu(OH)_2$. As for the laser-processed samples, Fig. 6 shows that the relative contribution of the components due to Cu(II) species in the Cu $2p_{3/2}$ signal tends to increase either with

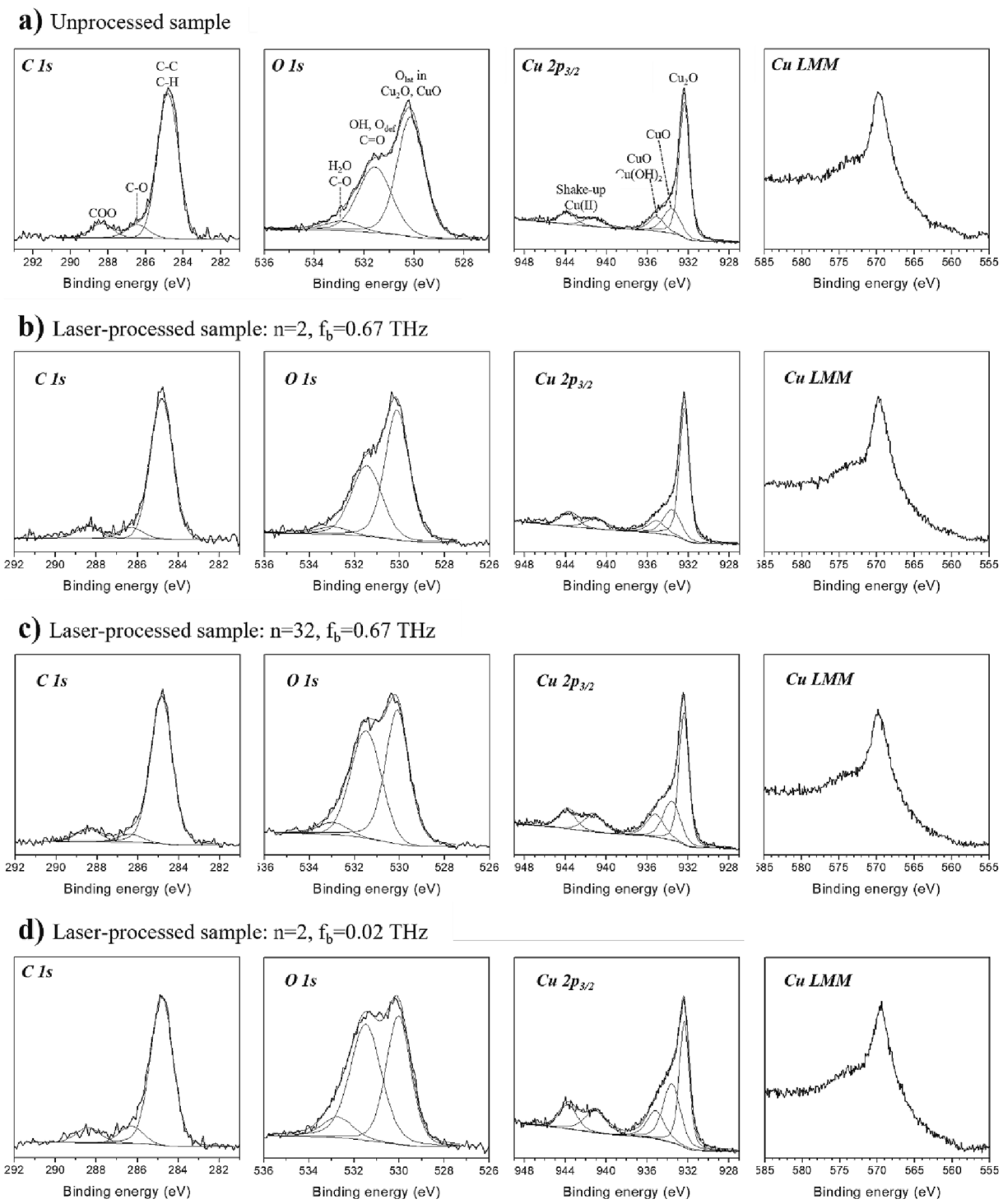

Fig. 6. High-resolution XPS C 1 s, O 1 s, Cu 2p3/2 and Cu LMM spectra of a) a thermal-treated unprocessed Cu sample and three thermal-treated laser-processed targets obtained with bursts of b) 2 sub-pulses @ 0.67 THz, c) 32 sub-pulses @ 0.67 THz, d) 2 sub-pulses @ 0.02 THz.

increasing the number of sub-pulses (Fig. 5c) or with decreasing the intra-burst frequency (Fig. 6d). In particular, curve-fitting results of the Cu $2p_{3/2}$ signal indicate that the XPS Cu(II)/Cu(I) ratio is *ca.* 45/55 for both the unprocessed and the 2sub-pulses@0.67THz processed samples, and increases to about 55/45 and 66/34 when bursts of 32 sub-pulses@0.67 THz and 2 sub-pulses@0.02 THz are used, respectively. This could be due to the increased presence of nanoparticles/nano-formations superimposed to LIPSS (Fig. 1), being richer in more oxidized Cu species, as also found in [45]. Moreover, longer bursts, i.e., bursts of 32 sub-pulses@0.67 THz and 2 sub-pulses@0.02 THz, also caused a detectable rise in the O 1 s spectrum, mainly consisting of an increase of the relative contribution of the component at 531.5 ± 0.2 eV (OH in Cu $(OH)_2$, defective oxygen, C = O groups) with respect to that of the peak at 530.3 ± 0.2 eV (lattice oxygen in Cu_2O and CuO) [42–44]. Indeed, due to the the lattice expansion occurring within the burst itself [11,38,39], a different reactivity of these surfaces could be exhibited, resulting in a favored formation on the targets of defective copper oxides and $Cu(OH)_2$ after the thermal treatment.

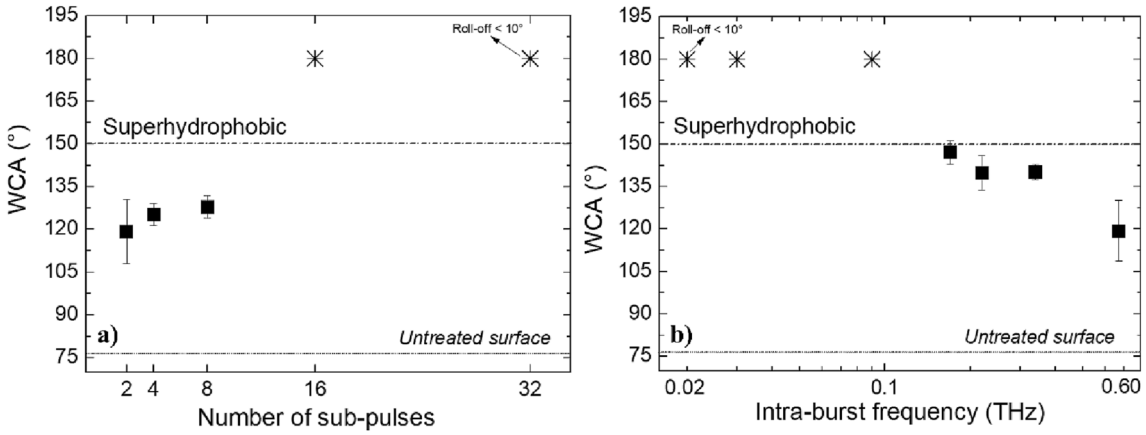

Fig. 7. Variation of water contact angle with a) the number of sub-pulses within the bursts (@ an intra-burst frequency of 0.67 THz) and b) the intra-burst frequency (with n = 2). The dotted line in a) and b) indicates the WCA of an unprocessed (thermallly treated) surface. The total fluence is set to 0.52 J/cm^2.

3.3. *Wettability of laser-bursts-processed copper targets*

The wetting response of the surfaces obtained with different burst configurations (at fixed total fluence) and followed by a thermal treatment was investigated by static contact angle (CA) measurements. The results are shown in Fig. 7.

In Fig. 7 a), it is clearly visible that the laser treatment with bursts, followed by low temperature annealing, caused the copper targets to acquire a hydrophobic behavior, although it is known that the thermal treatment is followed by the formation of chemical compounds (e.g., oxides) which rather would promote a higher wettability. In particular, the WCA goes from a value of 76° for an unprocessed thermally-treated sample to values between 119° (samples structured with 2-sub-pulses bursts with intra-burst frequency of 0.67 THz) and 127° (samples structured with 8-sub-pulses bursts with intra-burst frequency of 0.67 THz). In conventional normal pulse mode (NPM) irradiation [6,8], it was reported that a significant increase of the applied fluence (above 5 J/cm2) was necessary to inhibit wettability of copper and reach WCA above 150°. Conversely, Fig. 7 shows that, as long as the number of sub-pulses within the bursts was further increased to 16 and 32, BM processing in a low fluence regime (0.52 J/cm2) resulted in the samples displaying a superhydrophobic performance, the so-called fakir conditions, which is characterized by water droplets that do not adhere to the surface but rather roll off [46,47]. In this case, the conventional sessile drop method for the WCA measurement [46] cannot be exploited, since the droplet does not lay on the target surface. In such cases, a WCA value of 180° [3,46,48] is commonly assumed. These instances are pointed out as asterisks in Fig. 7 a) and b), in the region labelled as "Superhydrophobic". However, the roll-off angle was evaluated in this case, and a value lower than 10° was found, which further supported the description of the wetting response falling under a Cassie-Baxter regime.

A similar behavior can be observed in Fig. 7 b), where the WCA of copper surfaces structured with 2-sub-pulses bursts increases when the intra-burst frequency decreases. In particular, the water contact angle goes from 119° (samples structured with 2-sub-pulses bursts with intra-burst frequency of 0.67 THz) to 147° (samples structured with 2-sub-pulses bursts with intra-burst frequency of 0.017 THz). Also in this case, a further decrease of the intra-burst frequency within the 2 sub-pulses bursts gave the surfaces a *fakir-like* character.

Experiments performed at higher total fluences (up to 0.72 J/cm^2), confirmed such trends, with a general increase of the WCA (at a set burst configuration) due a to higher formation of nanofeatures, in perfect agreement with [8].

In Table 3, the influence of the burst configurations on the morphology, the surface chemistry and the wettability of the laser-treated surfaces are summarized.

Table 3
Summary of the evolution of morphological, compositional and wetting properties of the surfaces as related to the employed burst configuration.

Burst Configuration	Morphology	Composition	Wettability
n = 2 **f = 0.67 THz** **Burst Duration = 1.5 ps**	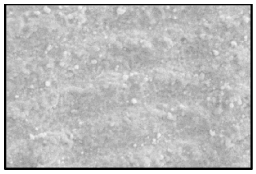	C (at %) = 43 ± 2O (at %) = 30 ± 2Cu (at %) = 27 ± 2	WCA = 119° ± 11°
n = 2 **f = 0.02 THz** **Burst Duration = 46.5 ps**	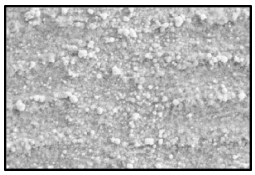	C (at %) = 41 ± 2O (at %) = 33 ± 2Cu (at %) = 26 ± 2	WCA = 180°
n = 32 **f = 0.67 THz** **Burst Duration = 46.5 ps**	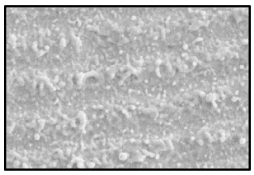	C (at %) = 43 ± 2O (at %) = 31 ± 2Cu (at %) = 26 ± 2	WCA = 180°

Though the increase of the CuO and $Cu(OH)_2$ relative contributions in the high-resolution XPS Cu $2p_{3/2}$ signal (Fig. 6) could suggest an increase of the wettability of the surfaces processed with n = 2@ 0.02 THz and n = 32 @ 0.67 THz, a shift from hydrophobic to superhydrophobic behavior is rather observed in Fig. 7.

The different wettability observed in this work can be ascribed to the different surface morphologies obtained wih the employed burst configurations. In fact, in section 3.1 we mentioned that the duration of the longest bursts, i.e., 32 sub-pulses@0.67 THz or 2 sub-pulses@0.02 THz, equal to 46.5 ps, is much longer than the electron–phonon coupling time in copper, i.e., 1–4 ps [37]. This causes the laser energy to be absorbed by the lattice already during the burst, thus leading to melting and, consequently, boosting the formation of nanoparticles/formations on top of the LSFL. In this way, it was possible to create a dual, hierarchical scale nanostructure, providing the surfaces with a highly water-repellent character [17].

Interestingly, in the present work the creation of such hierarchical topographies needed neither a double pass scanning strategy [49] or the use of high accumulated laser fluences [8,13,14,26]. Rather, it simply relied on a different distribution of the laser energy within the bursts, which has the potential to scale up laser-based fabrication speed through parallel processing, by fully exploiting the high repetition rates and high pulse energies of the laser sources.

4. Conclusions

In this work, surface structuring of copper targets was carried out with bursts of linearly polarized femtosecond laser pulses. Different burst features (number of sub-pulses within the bursts and intra-burst frequency) were explored, keeping the other processing parameters fixed, i.e., laser repetition rate, scan speed, hatch distance, total fluence, to highlight how the final surface properties are affected by the laser energy distribution within the bursts, in relation to the electron–phonon coupling time of copper, i.e., 1 – 4 ps. To this aim, the number of sub-pulses in the bursts was varied between 2 and 32, and their intra-burst frequency was set at 0.067 THz, thus generating bursts with different time duration, between 1.5 ps and 46.5 ps. Moreover, also bursts with only 2 sub-pulses with discrete variable intra-burst frequency (between 0.02 THz and 0.67 THz) were employed.

First of all, we found that the spatial periodicity of LSFL increased both as a function of the number of sub-pulses in the burst and of their time delay, in perfect agreement with one of our previous works [16], performed on steel. Moreover, it was also observed that LSFL were decorated by nanoparticles/nanoclusters whose appereance is generally related to thermal effects (melting) and was more likely when the the total burst duration was increased. Comparing the burst time duration with the electron–phonon coupling time, τ_{el}, it is possible to infer that for bursts with a duration comparable to or lower than τ_{el}, no lattice thermalization occurs within the burst itself, and the formation of such nanoparticles due to melting is less plausible. Conversely, when the burst duration is much longer than τ_{el}, lattice decomposition starts already during the bursts, causing lattice expansion and melting, thus making the generation of the nanoparticles/nanoclusters more likely [38].

An increase of the CuO and $Cu(OH)_2$ relative contributions in the high-resolution XPS Cu $2p_{3/2}$ signal (Fig. 6) was observed, which would suggest an increase of the wettability when n = 2@ 0.02 THz and n = 32 @ 0.67 THz. Instead, the wettability performances of some exemplary surfaces, evaluated by static water contact angle measurements, revealed that the presence of nanoparticles/nanoclusters superimposed to LSFL caused a shift towards superhydrophobic, antiadhesive behavior. Therefore, the transition from hydrophobic to superhydrohobic character, which we observed when increasing the burst duration, was mainly ascribed to the presence of the aforementioned nanoparticles decorating the LFL. In turn, this provided a double hierarchical scale to the surfaces, which therefore exhibited a highly water-repellent response [50].

In contrast with some previous works [8,49], our findings evidence that, in order to finely tune the copper wettability and render it superhydrophobic, increasing the laser fluence or using chemical compounds is not necessary, as long as the laser processing is carried out in burst mode. This suggests that low-fluence, high-speed parallel processing can be performed for structuring samples with large areas, thus efficiently exploiting the high repetition rates and high pulse energies of the current laser sources.

CRediT authorship contribution statement

Caterina Gaudiuso: Conceptualization, Methodology, Validation, Data curation, Visualization, Funding acquisition, Project administration, Writing – original draft, Writing – review & editing. **Fiorenza Fanelli:** Methodology, Validation, Investigation, Data curation, Visualization, Funding acquisition, Writing – original draft, Writing – review & editing. **Francesco Paolo Mezzapesa:** Validation, Writing – original draft. **Annalisa Volpe:** Writing – original draft. **Antonio Ancona:** Methodology, Supervision, Funding acquisition, Writing – review & editing.

Declaration of Competing Interest

The authors declare that they have no known competing financial interests or personal relationships that could have appeared to influence the work reported in this paper.

Data availability

Data will be made available on request.

Acknowledgements

The support to this work by the Apulian Region (Project FEB1B50F) and the Italian Ministry for University and Research (grant ARS01_00849) is gratefully acknowledged. C.G would thank Pietro Paolo Calabrese for his technical support and Vincenzo Scolletta for his experimental support.

References

[1] Z. Guo, W. Liu, B.L. Su, Superhydrophobic surfaces: From natural to biomimetic to functional, J. Colloid Interface Sci. 353 (2011) 335–355, https://doi.org/10.1016/j.jcis.2010.08.047.
[2] J. Drelich, E. Chibowski, D.D. Meng, K. Terpilowski, Hydrophilic and superhydrophilic surfaces and materials, Soft Matter 7 (2011) 9804–9828, https://doi.org/10.1039/c1sm05849e.
[3] A. Volpe, S. Covella, C. Gaudiuso, A. Ancona, Improving the laser texture strategy to get superhydrophobic aluminum alloy surfaces, Coatings 11 (2021) 1–12, https://doi.org/10.3390/coatings11030369.
[4] C. Putignano, G. Parente, F.J. Profito, C. Gaudiuso, A. Ancona, G. Carbone, Laser Microtextured Surfaces for Friction Reduction: Does the Pattern Matter ? Materials (Basel). 13 (2020) 4915, https://doi.org/10.3390/ma13214915.
[5] A.-M. Kietzig, S.G. Hatzikiriakos, P. Englezos, Patterned Superhydrophobic Metallic Surfaces, Langmuir 25 (2009) 4821–4827, https://doi.org/10.1021/la8037582.
[6] A.M. Kietzig, M.N. Mirvakili, S. Kamal, P. Englezos, S.G. Hatzikiriakos, Laser-patterned super-hydrophobic pure metallic substrates: Cassie to Wenzel wetting transitions, J. Adhes. Sci. Technol. 25 (2012) 2789–2809, https://doi.org/10.1163/016942410X549988.
[7] A.Y. Vorobyev, C. Guo, Multifunctional surfaces produced by femtosecond laser pulses, J. Appl. Phys. 117 (2015), https://doi.org/10.1063/1.4905616.
[8] E. Allahyari, J.J.J. Nivas, S.L. Oscurato, M. Salvatore, G. Ausanio, A. Vecchione, R. Fittipaldi, P. Maddalena, R. Bruzzese, S. Amoruso, Laser surface texturing of copper and variation of the wetting response with the laser pulse fluence, Appl. Surf. Sci. 470 (2019) 817–824, https://doi.org/10.1016/j.apsusc.2018.11.202.
[9] Y.E.B. Vidhya, A. Pattamatta, A. Manivannan, N.J. Vasa, Influence of fluence, beam overlap and aging on the wettability of pulsed Nd3+:YAG nanosecond laser-textured Cu and Al sheets, Appl. Surf. Sci. 548 (2021), 149259, https://doi.org/10.1016/j.apsusc.2021.149259.

[10] J. Bonse, S. Gräf, Ten open questions about laser-induced periodic surface structures, Nanomaterials 11 (2021) 1–21, https://doi.org/10.3390/nano11123326.

[11] G. Giannuzzi, C. Gaudiuso, R. Di Mundo, L. Mirenghi, F. Fraggelakis, R. Kling, P. M. Lugarà, A. Ancona, Short and long term surface chemistry and wetting behaviour of stainless steel with 1D and 2D periodic structures induced by bursts of femtosecond laser pulses, Appl. Surf. Sci. 494 (2019) 1055–1065, https://doi.org/10.1016/j.apsusc.2019.07.126.

[12] S. Kawabata, S. Bai, K. Obata, G. Miyaji, K. Sugioka, Two-dimensional laser-induced periodic surface structures formed on crystalline silicon by GHz burst mode femtosecond laser pulses, Int. J. Extrem. Manuf. 5 (2023), 015004, https://doi.org/10.1088/2631-7990/acb133.

[13] R. Liu, D. Zhang, Z. Li, Femtosecond laser induced simultaneous functional nanomaterial synthesis, in situ deposition and hierarchical LIPSS nanostructuring for tunable antireflectance and iridescence applications, J. Mater. Sci. Technol. 89 (2021) 179–185, https://doi.org/10.1016/j.jmst.2021.02.024.

[14] D. Zhang, C. Li, J. Xu, R. Liu, R. Duan, K. Feng, Z. Li, Higher Suitability of NbMoTaW over Its Elemental Metals for Laser Induced Periodic Surface Structure/Particle-Aggregate UV-to-MIR Ultrabroadband Absorber, Scr. Mater. 227 (2023), 115276, https://doi.org/10.1016/j.scriptamat.2023.115276.

[15] D. Zhang, R. Liu, Z. Li, Irregular LIPSS produced on metals by single linearly polarized femtosecond laser, Int. J. Extrem. Manuf. 4 (2022), https://doi.org/10.1088/2631-7990/ac376c.

[16] G. Giannuzzi, C. Gaudiuso, C. Di Franco, G. Scamarcio, P.M. Lugarà, A. Ancona, Large area laser-induced periodic surface structures on steel by bursts of femtosecond pulses with picosecond delays, Opt. Lasers Eng. 114 (2019) 15–21, https://doi.org/10.1016/j.optlaseng.2018.10.006.

[17] D. Huerta-Murillo, A. García-Girón, J.M. Romano, J.T. Cardoso, F. Cordovilla, M. Walker, S.S. Dimov, J.L. Ocaña, Wettability modification of laser-fabricated hierarchical surface structures in Ti-6Al-4V titanium alloy, Appl. Surf. Sci. 463 (2019) 838–846, https://doi.org/10.1016/j.apsusc.2018.09.012.

[18] E.Y. Bormashenko, Wetting of Real Surfaces (2013), https://doi.org/10.1515/9783110258790.

[19] C. Putignano, G. Parente, F.J. Profito, C. Gaudiuso, A. Ancona, G. Carbone, Laser microtextured surfaces for friction reduction: Does the pattern matter? Materials (Basel). 13 (2020) 1–21, https://doi.org/10.3390/ma13214915.

[20] J.M. Romano, A. Garcia-Giron, P. Penchev, S.S.S. Dimov, A.G. Giron, P. Penchev, S. S.S. Dimov, Triangular laser-induced submicron textures for functionalising stainless steel surfaces, Appl. Surf. Sci. 440 (2018) 162–169, https://doi.org/10.1016/j.apsusc.2018.01.086.

[21] S. Moradi, S. Kamal, P. Englezos, S.G. Hatzikiriakos, Femtosecond laser irradiation of metallic surfaces: Effects of laser parameters on superhydrophobicity, Nanotechnology 24 (2013), https://doi.org/10.1088/0957-4484/24/41/415302.

[22] D.V. Ta, A. Dunn, T.J. Wasley, R.W. Kay, J. Stringer, P.J. Smith, C. Connaughton, J. D. Shephard, Nanosecond laser textured superhydrophobic metallic surfaces and their chemical sensing applications, Appl. Surf. Sci. 357 (2015) 248–254, https://doi.org/10.1016/j.apsusc.2015.09.027.

[23] W. Liang, L. Zhu, W. Li, C. Xu, H. Liu, Facile Fabrication of Binary Nanoscale Interface for No-Loss Microdroplet Transportation, Langmuir 32 (2016) 5519–5525, https://doi.org/10.1021/acs.langmuir.6b01455.

[24] A. He, W. Liu, W. Xue, H. Yang, Y. Cao, Nanosecond laser ablated copper superhydrophobic surface with tunable ultrahigh adhesion and its renewability with low temperature annealing, Appl. Surf. Sci. 434 (2018) 120–125, https://doi.org/10.1016/j.apsusc.2017.10.143.

[25] D. Meena Narayana Menon, M. Giardino, D. Janner, Tunable pulsewidth nanosecond laser texturing: From environment friendly superhydrophobic to superamphiphobic surfaces, Appl. Surf. Sci. 610 (2023) 155356. 10.1016/j.apsusc.2022.155356.

[26] S. Sarbada, Y.C. Shin, Superhydrophobic contoured surfaces created on metal and polymer using a femtosecond laser, Appl. Surf. Sci. 405 (2017) 465–475, https://doi.org/10.1016/j.apsusc.2017.02.019.

[27] J. Mur, R. Petkovšek, Near-THz bursts of pulses – Governing surface ablation mechanisms for laser material processing, Appl. Surf. Sci. 478 (2019) 355–360, https://doi.org/10.1016/j.apsusc.2019.01.182.

[28] C. Gaudiuso, P.N. Terekhin, A. Volpe, S. Nolte, B. Rethfeld, A. Ancona, Laser ablation of silicon with THz bursts of femtosecond pulses, Sci. Rep. 11 (2021) 13321, https://doi.org/10.1038/s41598-021-92645-7.

[29] C. Gaudiuso, G. Giannuzzi, A. Volpe, P.M. Lugarà, I. Choquet, A. Ancona, Incubation during laser ablation with bursts of femtosecond pulses with picosecond delays, Opt. Express. 26 (2018) 3801, https://doi.org/10.1364/OE.26.003801.

[30] C. Gaudiuso, B. Stampone, G. Trotta, A. Volpe, A. Ancona, Investigation of the micro-milling process of steel with THz bursts of ultrashort laser pulses, Opt. Laser Technol. 162 (2023), 109301, https://doi.org/10.1016/j.optlastec.2023.109301.

[31] B. Dromey, M. Zepf, M. Landreman, K.O. Keeffe, T. Robinson, S.M. Hooker, Generation of a train of ultrashort pulses from a compact birefringent crystal array, Appl. Opt. 46 (2007) 5142–5146.

[32] S. Zhou, D. Ouzounov, H. Li, I. Bazarov, B. Dunham, C. Sinclair, F.W. Wise, Efficient temporal shaping of ultrashort pulses with birefringent crystals, Appl. Opt. 46 (2007) 8488–8492.

[33] C.V. Ngo, D.M. Chun, Fast wettability transition from hydrophilic to superhydrophobic laser-textured stainless steel surfaces under low-temperature annealing, Appl. Surf. Sci. 409 (2017) 232–240, https://doi.org/10.1016/j.apsusc.2017.03.038.

[34] A. Kietzig, M.N. Mirvakili, J. Adhesion Sci. Laser-Patterned Super- Hydrophobic Pure Metallic Substrates: Cassie Wenzel Wetting Transitions (2012) 2789–2809.

[35] S. Hou, Y. Huo, P. Xiong, Y. Zhang, S. Zhang, T. Jia, Z. Sun, J. Qiu, Z. Xu, Formation of long- and short-periodic nanoripples on stainless steel irradiated by femtosecond laser pulses, J. Phys. D. Appl. Phys. 44 (2011), https://doi.org/10.1088/0022-3727/44/50/505401.

[36] M. Charron, D. Poitras, J. Guay, A. Cala, L. Ramunno, P. Berini, A. Weck, Laser-induced plasmonic colours on metals (2017). 10.1038/ncomms16095.

[37] H.E. Elsayed-Ali, T.B. Norris, M.A. Pessot, G.A. Mourou, Time-resolved observation of electron-phonon relaxation in copper, Phys. Rev. Lett. 58 (1987) 1212–1215, https://doi.org/10.1103/PhysRevLett.58.1212.

[38] F. Fraggelakis, G. Mincuzzi, J. Lopez, I. Manek-hönninger, R. Kling, Applied Surface Science Controlling 2D laser nano structuring over large area with double femtosecond pulses, Appl. Surf. Sci. 470 (2019) 677–686, https://doi.org/10.1016/j.apsusc.2018.11.106.

[39] F. Fraggelakis, G. Giannuzzi, C. Gaudiuso, I. Manek-Hönninger, G. Mincuzzi, A. Ancona, R. Kling, Double- and Multi-Femtosecond Pulses Produced by Birefringent Crystals for the Generation of 2D Laser-Induced Structures on a Stainless Steel Surface, Materials (Basel). 12 (2019) 1257, https://doi.org/10.3390/ma12081257.

[40] S. Tardio, P.J. Cumpson, Practical estimation of XPS binding energies using widely available quantum chemistry software, Surf. Interface Anal. 50 (2018) 5–12, https://doi.org/10.1002/sia.6319.

[41] A. Samanta, Q. Wang, S.K. Shaw, H. Ding, Roles of chemistry modification for laser textured metal alloys to achieve extreme surface wetting behaviors, Mater. Des. 192 (2020), 108744, https://doi.org/10.1016/j.matdes.2020.108744.

[42] M.C. Biesinger, Advanced analysis of copper X-ray photoelectron spectra, Surf. Interface Anal. 49 (2017) 1325–1334, https://doi.org/10.1002/sia.6239.

[43] M.C. Biesinger, L.W.M. Lau, A.R. Gerson, R.S.C. Smart, Resolving surface chemical states in XPS analysis of first row transition metals, oxides and hydroxides: Sc, Ti, V, Cu and Zn, Appl. Surf. Sci. 257 (2010) 887–898, https://doi.org/10.1016/j.apsusc.2010.07.086.

[44] D. Barreca, A. Gasparotto, E. Tondello, CVD Cu2O and CuO Nanosystems Characterized by XPS, Surf. Sci. Spectra. 14 (2007) 41–51, https://doi.org/10.1116/11.20080701.

[45] D.W. Mu, A. Holtsch, S. Lo, C. Pauly, C. Spengler, S. Grandthyll, K. Jacobs, F. Mu, F. Mu, In-Depth Investigation of Copper Surface Chemistry Modi fi cation by Ultrashort Pulsed Direct Laser Interference Patterning, (2020). 10.1021/acs.langmuir.0c01625.

[46] D. Zhang, F. Chen, Q. Yang, J. Yong, H. Bian, Y. Ou, J. Si, X. Meng, X. Hou, A simple way to achieve pattern-dependent tunable adhesion in superhydrophobic surfaces by a femtosecond laser, ACS Appl. Mater. Interfaces. 4 (2012) 4905–4912, https://doi.org/10.1021/am3012388.

[47] M. Callies, D. Quéré, On water repellency, Soft Matter 1 (2005) 55–61, https://doi.org/10.1039/b501657f.

[48] J. Zhang, X. Gao, L. Jiang, Application of superhydrophobic edge effects in solving the liquid outflow phenomena, Langmuir 23 (2007) 3230–3235, https://doi.org/10.1021/la063006w.

[49] Q. Wang, K. Yin, Z. Bai, J. Liu, L. Huo, H. Wang, Fabrication of robust superhydrophobic copper surface via highly efficient nanosecond laser-based surface functionalization, Optik (Stuttg). 276 (2023), 170690, https://doi.org/10.1016/j.ijleo.2023.170690.

[50] J.T. Cardoso, A.I. Aguilar-Morales, S. Alamri, D. Huerta-Murillo, F. Cordovilla, A. F. Lasagni, J.L. Ocaña, Superhydrophobicity on hierarchical periodic surface structures fabricated via direct laser writing and direct laser interference patterning on an aluminium alloy, Opt. Lasers Eng. 111 (2018) 193–200, https://doi.org/10.1016/j.optlaseng.2018.08.005.